A Unifying Approach to Registration, Segmentation, and Intensity Correction

Kilian M. Pohl[1], John Fisher[1], James J. Levitt[2], Martha E. Shenton[2], Ron Kikinis[2], W. Eric L. Grimson[1], and William M. Wells[2]

[1] Computer Science and Artificial Intelligence Lab, Massachusetts Institute of Technology, Cambridge, MA, USA, {pohl,fisher,welg}@csail.mit.edu

[2]Surgical Planning Laboratory, Harvard Medical School and Brigham and Women's Hospital, Boston, MA, USA, {jlevitt,martha,kikinis,sw}@bwh.harvard.edu

Abstract. We present a statistical framework that combines the registration of an atlas with the segmentation of magnetic resonance images. We use an Expectation Maximization-based algorithm to find a solution within the model, which simultaneously estimates image inhomogeneities, anatomical labelmap, and a mapping from the atlas to the image space. An example of the approach is given for a brain structure-dependent affine mapping approach. The algorithm produces high quality segmentations for brain tissues as well as their substructures. We demonstrate the approach on a set of 22 magnetic resonance images. In addition, we show that the approach performs better than similar methods which separate the registration and segmentation problems.

1 Introduction

With notable exceptions, segmentation and registration have been treated as two separate problems in medical imaging research. However, these techniques complement each other. For example, segmentation simplifies the registration of anatomical structures with ambiguous intensity patterns [1]. On the other hand, aligning an atlas to these anatomical structures aids the detection of indistinct boundaries and therefore simplifies the segmentation problem [2]. In this paper, we describe a simultaneous solution to both problems by combining them in a unified Bayesian framework.

The idea of the unified Bayesian framework was motivated by boundary localization techniques, such as [3, 4], which align an atlas to the subject and simultaneously estimate the shape of a structure. These methods relate both problems to each other by extending the definition of the shape to include its pose. This paper describes an integrated segmentation and registration approach for voxel-based classification methods. In contrast to boundary localization approaches, voxel-based classification methods consider the anatomical structure associated with each voxel. In addition, they often explicitly model the image inhomogeneities of Magnetic Resonance Images (MRI) to segment large data sets without manual intervention.

Voxel-based classification methods have coupled registration and segmentation of misaligned images [5, 6], however, we wish to align an atlas to MRI and separate the images into anatomical structures. Previous voxel-based classification methods perform this task sequentially [7, 8, 2] increasing the risk of systematic biases [1]. In contrast, our new approach is based on the principle of least commitment so that an initial imperfect estimation converges to a good approximation for each problem.

Similar to [8, 9, 1], this paper is based on an instance of the Expectation Maximization Algorithm (EM) using non-stationary priors to outline structures with indistinct boundaries and to estimate image inhomogeneities. Instead of *sequentially* performing registration and segmentation [8, 9, 1], we propose in Section 2 a Bayesian framework

describing the relationship between atlas registration, intensity correction, and image segmentation. This framework is based on a Maximum A posteriori Probability (MAP) estimation formulation approximating the solution to these three interrelated problems.

Section 3 applies the concept to a hierarchical registration framework modeling global- and structure-dependent deformations. The limits and benefits of the implementation are illustrated in Section 4 by presenting a study comparing the robustness of our algorithm with respect to other EM implementations. In this study, the automatic methods outline a set of 22 MRIs into the major brain tissue classes as well as the thalamus and caudate, which are structures with indistinct boundaries.

2 Deriving an EM Framework for Simultaneous Inhomogeneity Correction, Registration, and Segmentation

The accuracy of segmenting structures that have indistinct boundaries on MR images with tissue classification methods significantly depends on properly modeling the image inhomogeneities as well as correctly registering the atlas to the subject. In this section, we develop a unified framework which performs segmentation, registration and inhomogeneity correction simultaneously.

2.1 A Maximum a Posteriori Probability Estimation Problem

Due to their complex dependencies, it is very difficult to extract the inhomogeneities $\mathcal{B}$ and the registration parameters $\mathcal{R}$ from the MRI I without the explicit knowledge of the unknown true segmentation. However, this problem is greatly simplified within an EM framework where it is formulated as an incomplete data problem marginalizing over all possible segmentations $\mathcal{T}$. To determine $\mathcal{B}$ and $\mathcal{R}$ within this framework, we define the following MAP estimation problem over the incomplete data model:

$$(\hat{\mathcal{B}}, \hat{\mathcal{R}}) = \arg\max_{\mathcal{B},\mathcal{R}} \log P(\mathcal{B}, \mathcal{R} | I). \tag{1}$$

In general, this results in a system of equations for which there is no analytical solution.

To estimate a solution for this problem, we propose an EM model that improves the initial estimate $(\mathcal{B}', \mathcal{R}')$ by solving the following MAP estimation problem:

$$(\mathcal{B}', \mathcal{R}') \leftarrow \arg\max_{\mathcal{B},\mathcal{R}} E_{\mathcal{T}|I,\mathcal{B}',\mathcal{R}'} (\log P(I|\mathcal{T}, \mathcal{B}) + \log P(\mathcal{R}|\mathcal{T}) + \log P(\mathcal{B})) \tag{2}$$

The relationship between Equation (1) and Equation (2) is described in detail in our technical report [10]. This report shows that the update rule of Equation (2) yields a better estimate of $(\mathcal{B}', \mathcal{R}')$ as measured by Equation (1). In addition, this EM framework guarantees convergence to a local maxima of the objective function [11].

Based on the derivation of [10], the solution of Equation (2) improves $(\mathcal{B}', \mathcal{R}')$ by iterating between the Expectation-Step (E-Step) and Maximization-Step (M-Step). The E-Step calculates the posterior of an anatomical structure a with respect to voxel x

$$\mathcal{W}'_x(a) = \frac{P(I_x|\mathcal{T}_x = e_a, \mathcal{B}'_x) \cdot P(\mathcal{T}_x = e_a|\mathcal{R}')}{P(I_x|\mathcal{B}'_x, \mathcal{R}')} \tag{3}$$

with $\mathcal{T}_x$ being the indicator random vector at voxel x. e_a is zero but at position a, where it is one. The M-Step updates the estimates by solving the following two MAP problems

$$\mathcal{R}' \leftarrow \arg\max_{\mathcal{R}} \sum_x \sum_a \mathcal{W}'_x(a) \cdot \log P(\mathcal{T}_x = e_a|\mathcal{R}) + \log P(\mathcal{R}) \tag{4}$$

$$\mathcal{B}' \leftarrow \arg\max_{\mathcal{B}} \sum_x \sum_a \mathcal{W}'_x(a) \cdot \log P(I|\mathcal{T}_x = e_a, \mathcal{B}) + \log P(\mathcal{B}) \tag{5}$$

A variety of closed-form solutions for Equation (5) have been proposed in the literature such as [8] and [12].

The remainder of this paper focuses on modeling Equation (4). Before doing so we must point the method's sensitivity towards uncommon characteristics favored by the atlas; a minor drawback of this formulation. The aligned atlas is represented in Equation (4) and Equation (3) by $P(\mathcal{T}_x = e_a|\mathcal{R})$. To match the atlas with the segmentation weights, the algorithm compensates for any biases through intensity correction and atlas realignment. For example, if the atlas does not properly capture the brain intensity distribution, the algorithm might identify the neck as part of the brain. The inhomogeneity correction will then normalize the intensity pattern of the neck to the once inside the brain and the registration might scale the atlas of the brain to cover both brain and neck. This causes the algorithm to converge to a suboptimal solution but a re-calibration of the atlas to the intensity pattern of the MRI protocol can overcome this problem.

In summary, we find a local maxima to the difficult MAP problem of Equation (1) by solving it within an EM framework. The E-Step determines $\mathcal{W}$ of Equation (3) and the M-Step solves for the MAP estimates specified by Equation (4) and Equation (5).

2.2 Defining a Hierarchical Registration Approach

To solve the MAP estimation problem of Equation (4), we define the registration parameters $\mathcal{R}$, $\log P(\mathcal{T}|\mathcal{R})$, and $P(\mathcal{R})$. The parameters $\mathcal{R}$ model a hierarchical registration framework, which distinguishes between global- and structure-dependent deformations. We then apply the registration framework to the MAP estimation problem and find a solution with another optimization algorithm.

The hierarchical registration parameters $\mathcal{R}$ capture the correspondence between atlas, brain, and structures within the brain. The parameters $\mathcal{R}$ can be structure-dependent or -independent. Structure-independent parameters capture the correspondence between atlas and image space. When limited to affine interpolation, the degrees of freedom of $\mathcal{R}$ are too low to capture the characteristics of individual brain structures ([13]). The alternative is a more general non-rigid framework which often has problems aligning structures with indistinct boundaries [1].

Our Structure-dependent registration parameters treat the relationship between atlas and image space for each structure independently. Since most of the misalignment is structure-independent, e.g the patient's head is not aligned with the atlas space, we expect small differences between structure-dependent parameters of different structures. We model this dependency with a hierarchical registration framework $\mathcal{R} = (\mathcal{R}_G, \mathcal{R}_S)$. $\mathcal{R}_G$ are the global registration parameters, which describe the non-structure dependent deformations between atlas and image. $\mathcal{R}_S \triangleq (\mathcal{R}_1, \ldots, \mathcal{R}_N)$ are the structure dependent parameters of structure $1, \ldots, N$, which represent the residual structure-specific deformations not adequately explained by $\mathcal{R}_G$. The similarity between structure specific parameters is encoded in Equation (4) through the prior probability $P(\mathcal{R})$ enforcing tight bounds on $\mathcal{R}_S$ and weak constraints on $\mathcal{R}_G$.

The mapping of the atlas to the image space is performed by an interpolation function $r(\mathcal{R}_G, \mathcal{R}_a, x)$, which maps voxel x into the coordinate system of structure a. Unlike global affine registration methods, this results in structure dependent coordinate systems represented by $(r(\mathcal{R}_G, \mathcal{R}_1, \cdot), \ldots, r(\mathcal{R}_G, \mathcal{R}_N, \cdot))$ that are not aligned with each other.

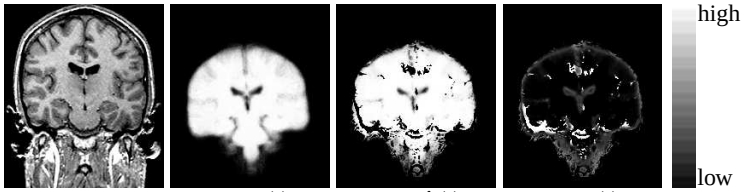

(a) MRI (b) $f_a(\cdot)$ (c) $\mathcal{W}_a(\cdot)$ (d) $Q(\cdot)$

Fig. 1. Image (a) shows an MRI, which is segmented by our EM implementation using the misaligned spatial atlas of the brain $f_a(\cdot)$ in (b). $\mathcal{W}$ in (c) is the result of E-Step and $Q(\cdot)$ in (d) is the initial cost function of the M-Step. $Q(\cdot)$ measures the disagreement between $f_a(\cdot)$ and $\mathcal{W}_a(\cdot)$ with black indicating agreement and white showing disagreement between the two instances.

Let $\mathcal{R}_a$ of $\mathcal{R}_S$ be the parameters specific to structure a with $a \in \{1,\ldots,N\}$. If we define f_a as the probability over voxel location in the atlas space conditioned on structure a then $f_a\left(r(\mathcal{R}_G,\mathcal{R}_a,\cdot)\right)$ is defined in the structure specific coordinate system of the patient. Thus, we can model the conditional structure probability:

$$P(\mathcal{T}_x = e_a|\mathcal{R}) \triangleq \frac{f_a\left(r(\mathcal{R}_G,\mathcal{R}_a,x)\right)}{\sum_{a'} f_{a'}\left(r(\mathcal{R}_G,\mathcal{R}_{a'},x)\right)} \tag{6}$$

Substituting Equation (6) into Equation (4) changes the MAP problem to

$$\begin{aligned}\mathcal{R}' \leftarrow \arg\max_{\mathcal{R}} \sum_x \sum_a \left[\mathcal{W}_x(a)\cdot\left(\log f_a[r(\mathcal{R}_G,\mathcal{R}_a,x)] - \log\textstyle\sum_{a'} f_{a'}[r(\mathcal{R}_G,\mathcal{R}_{a'},x)]\right)\right] \\ + \log P(\mathcal{R}) = \arg\max_{\mathcal{R}} Q(\mathcal{R})\end{aligned} \tag{7}$$

where the objective function $Q(\cdot)$ of Equation (7) is defined as

$$Q(\mathcal{R}) \triangleq \sum_x \sum_a \mathcal{W}_x(a)\cdot\log(f_a\left[r(\mathcal{R}_G,\mathcal{R}_a,x)\right]) - \log\left(\textstyle\sum_a f_a\left[r(\mathcal{R}_G,\mathcal{R}_{a'},x)\right]\right) + \log P(\mathcal{R}) \tag{8}$$

$Q(\cdot)$ measures the disagreement between between $f_a(\cdot)$ and $\mathcal{W}_a(\cdot)$ (see Figure 1.) One can also show that $Q(\cdot)$ relates to the Kullback-Leibler divergence. The objective function is therefore maximized with respect to $\mathcal{R}$ if $f_a(r(\mathcal{R}_G,\mathcal{R}_a,x))$ is made as close as possible to $\mathcal{W}_x(a)$. For example, if voxel x is clearly assigned to structure a' with $y_a \triangleq r(\mathcal{R}_G,\mathcal{R}_a,x)$ being the coordinate of voxel x in the atlas space of structure a then $\mathcal{W}_x(a') = 1$ and $f_{a'}(y_{a'}) = \sum_a f_a(y_a)$. The value of the sum across all structures of Equation (8) at x is zero as

$$\textstyle\sum_a \left[\mathcal{W}_x(a)\log(f_a(y_a)\right] - \log(f_{a'}(y_{a'})) = \log(f_{a'}(y_{a'})) - \log(f_{a'}(y_{a'})) = 0.$$

In summary, we developed a hierarchical registration framework guided by global and structure specific deformations. We transformed Equation (4) into Equation (7), whose objective function $Q(\cdot)$ measures the disagreement between the current alignment of the atlas space and the segmentation weights.

3 Affine Registration Implementation

This section describes an implementation of the approach presented in Section 2.2. We will give an example of an interpolation function $r(\cdot,\cdot,\cdot)$, the corresponding registration parameters $\mathcal{R}$, a Probability Density Function (PDF) $P(\mathcal{R})$, and a maximization algorithm to solve the MAP problem defined in Equation (7).

The interpolation function $r(\cdot,\cdot,\cdot)$ of Section 2 can model various mapping approaches. For simplicity, we choose an affine interpolation so that $\mathcal{R}_z = (\overrightarrow{t_z}^t, \overrightarrow{r_z}^t, \overrightarrow{s_z}^t)^t$ with $z \in \{G,1,\ldots,N\}$ define displacement $\overrightarrow{t_z}$, rotation $\overrightarrow{r_z}$, and scaling $\overrightarrow{s_z}$. The mapping

is defined as $r(\cdot,\cdot,\cdot) : \mathbb{R}^{12\times12\times3} \rightarrow \mathbb{R}^3, (\mathcal{R}_G, \mathcal{R}_a, x) \rightarrow A_{\mathcal{R}_G} \cdot A_{\mathcal{R}_a} \cdot (x^t, 1)^t$ where $A_{\mathcal{R}_z}$ is an affine transformation matrix based on the parameter setting $\mathcal{R}_z$.

We do not assume correspondence between the atlas and the image space so that we choose a uniform prior for the global registration parameter $\mathcal{R}_G$. As opposed to $\mathcal{R}_G$, the structure specific parameters $\mathcal{R}_S \triangleq (\mathcal{R}_1, \ldots, \mathcal{R}_N)$ describe the residual of structure specific deformations that are not well explained by $\mathcal{R}_G$. In general, our model should penalize large deviations of $\mathcal{R}_S$ from the expected mean, which is approximated by the average structure-specific registration parameters of the training data. We enforce this penalty by modeling the PDF of $\mathcal{R}_S$ as a Gaussian distribution $N(\mu_{\mathcal{R}_S}, \Upsilon_{\mathcal{R}_S})$ with structure independent mean $\mu_{\mathcal{R}_S}$ and variance $\Upsilon_{\mathcal{R}_S}$ based on the mapping parameters of the training data. We choose a Gaussian distribution as small variance $\Upsilon_{\mathcal{R}_S}$ discourages large deformations from the mean $\mu_{\mathcal{R}_S}$. In addition, Gaussian distributions simplify the calculations in the M-Step [11].

Based on the previous modeling assumptions the objective function is defined as

$$Q(\mathcal{R}) \triangleq \sum_x \Big(\sum_a \big(\mathcal{W}_x(a) \cdot \log \big[f_a(A_{\mathcal{R}_G} \cdot A_{\mathcal{R}_a} \cdot (x^t, 1)^t) \big] \big) - \log \big[\sum_a f_a(A_{\mathcal{R}_G} \cdot A_{\mathcal{R}_a} \cdot (x^t, 1)^t) \big] \Big) - \frac{1}{2} (\mathcal{R}_S - \mu_{\mathcal{R}_S})^t \Upsilon_{\mathcal{R}_S}^{-1} (\mathcal{R}_S - \mu_{\mathcal{R}_S}).$$

Determining a closed form solution to the MAP problem defined by $Q(\cdot)$ is difficult. Instead, we estimate the solutions through the Powell's method [14]. We also decouple the search for $\mathcal{R}_G$ and $\mathcal{R}_S$ as their dependencies can cause instability. The pseudo code for this implementation is given below.

Algorithm 1: SEGMENTATION AND REGISTRATION()

repeat
  E-Step: Update soft assignment of anatomical structures
    $\mathcal{W}_x(a) \leftarrow \frac{1}{Z} P(I_x | \mathcal{T}_x = e_a, \mathcal{B}'_x) \cdot f_a\left(r(\mathcal{R}'_G, \mathcal{R}'_a, x)\right)$
  M-Step: Update parameter space
    $\mathcal{B}' \leftarrow$ Estimation of the image inhomogeneities based on $\mathcal{W}$
    $\mathcal{R}'_G \leftarrow$ Result of Powell's method with $Q((\cdot, \mathcal{R}'_S))$
    $\mathcal{R}'_S \leftarrow$ Result of Powell's method with $Q((\mathcal{R}'_G, \cdot))$
until $\mathcal{B}'$ and $\mathcal{R}'$converge
define labelmap: $\mathcal{T}_x \leftarrow \arg\max_a \mathcal{W}_x(a)$

4 Comparative Experiment on 22 Test Cases

The section compares three EM methods which differ in the mapping of the atlas to the patient. The first approach (EM-NonRigid) aligns the atlas using an intensity based non-rigid registration approach and then runs our EM implementation without registration parameters [1]. The second approach (EM-Affine) is similar to EM-NonRigid but uses the affine mapping method by [15] as the preprocessing step. The third approach (EM-Integrated) is our new algorithm solving registration and segmentation simultaneously. All three methods use the same atlas which was generated according to [1]. In order to compare the three methods, each of them segments 22 test cases into the three brain tissue classes and further parcellates grey matter into the subcortical structures thalamus and caudate. We then measure the agreement of the automatic segmentations of the subcortical structures to manual ones, which we view as ground-truth.

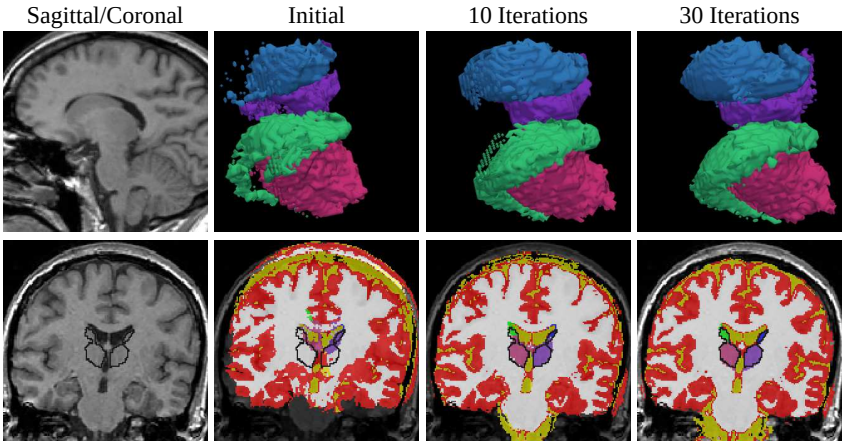

Fig. 2. The top row shows an MRI with unusual head position and the corresponding 3D models of our segmentations of the thalamus and caudate. The button row shows the coronal MRI with black indicating the two manually outlined structures. The segmentations to the left are produced by our method, which initial performs poorly but converges closely to the experts' results.

This experiment focuses on the thalamus and caudate as they are challenging structures for registration and segmentation. Purely intensity based methods, such as EM without spatial priors, cannot segment these structures because part of the boundary is invisible on MRI (Figure 3). Consequently, EM relies heavily on spatial priors making it sensitive towards misaligned priors. The registration of the priors is also a challenge. Intensity based alignment methods, such as [16], have difficulties mapping the priors to the thalamus because of the structure's similar intensity properties to the adjacent white matter; affine registration methods, such as [15], are too constrained to properly capture the bending within the horn-shaped caudate. In conclusion, a detailed analysis of the segmentation of thalamus and caudate highlights the differences between the three methods.

To measure the quality of the automatic generated results, we compare them to the manual segmentations of the thalamus and caudate using the Dice volume overlap measure. The graph in Figure 3 shows the mean and standard error of the Dice measure for the three algorithms. For the thalamus, EM-NonRigid (NRigid) performed worst because the intensity based registration method is too unreliable for structures with smooth boundaries. The method often overestimates white matter and underestimated the thalamus in this region (Figure 3(EM-NonRigid)). EM-Affine (Affine) performs much better than EM-NonRigid but the method is sensitive towards initial misalignments. For example, EM-Affine cannot properly address the unusual pose of the patient in Figure 2 (Sagittal) causing a bias in the segmentation (Figure 3 (EM-Affine)).

For the caudate, EM-NonRigid performs much better than EM-affine. In contrast to the thalamus, the caudate has a different intensity profile than white matter. Only the relatively small portion of the boundary neighboring the putaman, another subcortical structure, is invisible on MRI. Thus, the intensity based registration method of EM-NonRigid correctly registers the spatial priors to this region. However, the affine registration method of EM-Affine does not have enough degrees of freedom to cap-

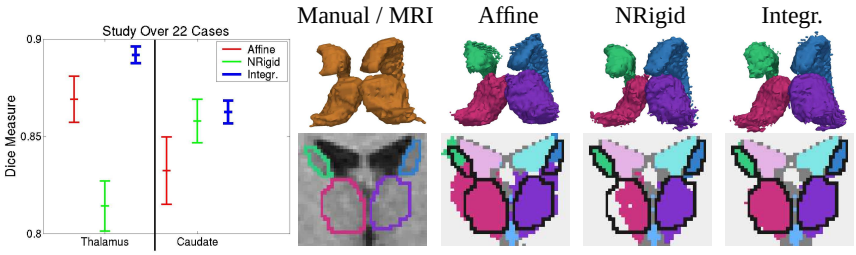

Fig. 3. The graph shows the mean and standard error of the three methods segmenting the thalamus and caudate in 22 cases. For both structures, our new approach EM-Integrated (Integr.) outperformed EM-Affine (Affine) and EM-NonRigid (NRigid). The segmentations to the right highlight deficiencies of EM-Affine and EM-NonRigid, such as the general underestimation of the thalamus by EM-NonRigid and the misalignment of the caudate by EM-Affine due the low degree of freedom. In the MRI as well as 2D segmentations the thalamus is outlined in black.

ture the patient specific bending of the horn-shaped caudate. This causes EM-Affine to misclassify voxels especially at the tip of the structure, which explains the lower score.

EM-Integrated (Integr.) generally outperformed the other two methods (Figure 3). For the thalamus, the method was significantly more reliable than the other two methods (mean Dice and standard error of EM-Integrated : $89.2 \pm 0.4\%$, EM-Affine: $86.9 \pm 1.2\%$, EM-NonRigid: $81.4 \pm 1.3\%$). For the caudate, EM-Integrated ($86.3 \pm 0.6\%$) was still significantly better than EM-Affine ($83.2 \pm 1.7\%$), but only slightly more robust than EM-NonRigid ($85.8 \pm 1.1\%$). However, the standard error of EM-Integrated is lower than EM-NonRigid indicating a higher predictive power of our new approach.

Our new approach performed much better than the two other method on cases, where the deformation between atlas and image space was complex. As the example of Figure 2 illustrates the accuracy of registration and segmentation greatly depend on each other. Initially, the algorithm only correctly outlines corticospinal fluid, whose disposition between the atlas and image space guides the registration (see also Figure 1(d)). As the method progresses, the overall accuracy of the registration as well as segmentation increases. In this example it took 30 iterations until the algorithm converged and correctly segmented the subcortical structures whose boundary is outlined in black.

We have demonstrated that our method performs better than EM-Affine and EM-NonRigid as a consequence that our approach directly maps the spatial priors of the structures to the segmentation model. In contrast, EM-Affine and EM-NonRigid align an MRI in the atlas space to the image of the patient, using the resulting deformation map to align the spatial priors. This inherently increases the risk of systematic biases in the model. Another explanation for the increased accuracy of our approach is the explicit modeling of dependency between segmentation and registration, which constrains the space of possible solutions and thus simplifies the segmentation problem.

5 Conclusion

We have presented a statistical framework combining inhomogeneity estimation, atlas registration, and segmentation of MRI. Unlike other voxel-based classification methods, our framework models these three problems as a single MAP estimation problem. We implemented the framework as an instance of an EM algorithm using a hierarchical affine mapping approach for anatomical structures. Our approach was validated by automatically segmenting 22 sets of MRIs into the major brain tissue classes and the sub-

cortical structures thalamus and caudate that are structures with indistinct boundaries. Using manual segmentations, we then compared our results to other EM implementations which sequentially register and segment. In general, our method performed much better than the other segmentation methods. The improvement is due primarily to the seamless integration of registration into the performance estimation problem.

Acknowledgments: This investigation was supported by the Department of Veterans Affairs (VA Merit Awards and a REAP Award), and NIH grants K02 MH-01110, R01 MH-50747, R01-NS051826-01, P41 RR-13218, U24 RR021382, and U54-EB-005149. We would also like to thank Corey Kemper, Sylvain Bouix, and Polina Golland for their helpful comments.

References

1. K. Pohl, S. Bouix, R. Kikinis, and W. Grimson, "Anatomical guided segmentation with non-stationary tissue class distributions in an expectation-maximization framework," in *ISBI*, pp. 81–84, 2004.
2. B. Fischl, D. Salat, E. Busa, M. Albert, M. Dieterich, C. Haselgrove, A. van der Kouwe, R. Killiany, D. Kennedy, S. Klaveness, A. Montillo, N. Makris, B. Rosen, and A. Dale, "Whole brain segmentation: Automated labeling of neuroanatomical structures in the human brain," *Neuron*, vol. 33, 2002.
3. M. Leventon, W. Grimson, and O. Faugeras, "Statistical shape influence in geodesic active contours," in *CVPR*, pp. 1316 – 1323, 2000.
4. A. Tsai, A. Yezzi, W. Wells, C. Tempany, D. Tucker, A. Fan, W. Grimson, and A. Willsky, "A shape-based approach to the segmentation of medical imagery using level sets," *TMI*, vol. 22, no. 2, pp. 137 – 154, 2003.
5. P. P. Wyatt and J. A. Noble, "MAP MRF joint segmentation and registration," in *MICCAI*, pp. 580–587, 2002.
6. C. Xiaohua, M. Brady, and D. Rueckert, "Simultaneous segmentation and registration for medical image," in *MICCAI*, pp. 663–670, 2004.
7. C. Cocosco, A. Zijdenbos, and A. Evans, "A fully automatic and robust brain MRI tissue classification method," *MIA*, vol. 7, pp. 513–527, 2003.
8. K. Van Leemput, F. Maes, D. Vanermeulen, and P. Suetens, "Automated model-based bias field correction of MR images of the brain," *TMI*, vol. 18, no. 10, pp. 885–895, 1999.
9. J. Marroquin, B. Vemuri, S. Botello, F. Calderon, and A. Fernandez-Bouzas, "An accurate and efficient bayesian method for automatic segmentation of brain MRI," *TMI*, vol. 21, 2002.
10. K. Pohl, J. Fisher, W. Grimson, and W. Wells, "An expectation maximization approach for integrated registration, segmentation, and intensity correction,", AIM-2005-010, CSAIL - MIT.
11. G. McLachlan, T. Krishnan, *The EM Algorithm and Extensions*. John Wiley & Sons, 1997.
12. W. Wells, W. Grimson, R. Kikinis, and F. Jolesz, "Adaptive segmentation of MRI data," *TMI*, vol. 15, pp. 429–442, 1996.
13. S. Srivastava, F. Maes, D. Vandermeulen, W. V. Paesschen, P. Dupont, and P. Suetens, "Effects of anatomical asymmetry in spatial priors on model-based segmentation of the brain MRI: A validation study," in *MICCAI*, no. 3216 in LNCS, pp. 327–334, Springer, 2004.
14. W. Press, B. Flannery, S. Teukolsky, and W. Vetterling, *Numerical Recipes in C : The Art of Scientific Computing*. Cambridge University Press, 2 ed., 1992.
15. S. Warfield, J. Rexilius, P. Huppi, T. Inder, E. Miller, W. Wells, G. Zientara, F. Jolesz, and R. Kikinis, "A binary entropy measure to assess nonrigid registration algorithm," in *MICCAI*, pp. 266–274, 2001.
16. A. Guimond, A. Roche, N. Ayache, and J. Meunier, "Three-dimensional multimodal brain warping using the demons algorithm and adaptive intensity corrections," *TMI*, vol. 20, 2001.